Coherent Transition Radiation-Based Diagnosis of Electron Beam Pulse Shape[1]

J.B.Rosenzweig, A. Murokh and A. Tremaine
Department of Physics and Astronomy
University of California, Los Angeles
Los Angeles, CA 90095

Abstract. The bunch shapes of an electron beams is increasingly difficult to measure, as the time-scales of interest are now sub-picosecond. We discuss here the use of coherent transition radiation CTR for such measurements. Two types of measurements are presented: the deduction of macroscopic (0.3 psec resolution) pulse profile using interferometry, and the examination of microbunch (50 fsec) structure from an FEL-bunched beam using spectral characteristics of the CTR. For the macrobunch measurement we discuss the problem of missing low frequency radiation and one solution for extracting meaningful data with this problem present. For microbunch CTR, we examing initial spectrally--resolved measurements, and some interesting deviations in the CTR spectrum from the standard theoretical predictions.

INTRODUCTION

The standard time-domain approaches to ultra-short electron beam pulse length diagnosis, such as streak cameras and rf sweeping, are inadequate when dealing with applications such as advanced accelerators and short-wavelength free-electron lasers (FELs). In order to move paset the picosecond level of resolution, it is necessary to use other methods. Coherent transition radiation (CTR) is one of the most promising of these methods. Much effort has been recently devoted to characterization of CTR itself[1], as well as performance of the actual bunch length measurements. This measurement is often done by examination of the autocorrelation of the CTR signal with the Michelson interferometer[2], which allows one to obtain the amplitude of the

[1] This work was supported by U.S. Dept. of Energy grants DE-FG03-93ER40796 and DE-FG03-92ER40693, and the Alfred P. Sloan Foundation grant BR-3225.

CP472, Advanced Accelerator Concepts: Eighth Workshop,
edited by W. Lawson, C. Bellamy, and D. Brosius

beam current's Fourier Transform. Direct spectral measurements of mm-wave CTR[3], as well as coherent synchrotron radiation[4] has also been performed.

We at UCLA have implemented two versions of a CTR-based pulse length diagnostic. The first is an interferometric device which allows the autocorrelation of the pulse to be obtained. This technique has certain limitations, as for beams of a few picosecond in length, the bunch length structure information is being mostly carried in the long wavelengths which are hard to propagate and detect with full efficiency. These most informative frequencies dominating the signal spectrum are in fact strongly attenuated in the collection optics due to the finite apertures and acceptance angles. This distortion of the detected spectrum puts a great uncertainty on the beam shape in the frequency domain, and makes the analysis rather difficult. To compensate for the missing frequencies an analytical method has been developed, which allows the processing of the autocorrelation signal directly in the time domain. Even though the frequency and time domains are equally representative to the signal, the accuracy of interpretation is increased drastically, as this analysis does not require that the autocorrelation signal be processed by discrete Fourier transform.

The second CTR-based method is a spectral approach used to obtain information concerning the beam microbunching as it is manifested in an FEL or an advanced accelerator[5]. We will discuss some details of initial measurements with this method, and some unexpected physical features found in these experimental data.

TRANSITION RADIATION DUE TO A SINGLE PARTICLE

In order to understand well the experimental measurements, we must first begin with a review of the relevant components of the theory of transition radiation and its coherent generation by short bunches of electrons. The process of a charged particle crossing the boundary of the perfect conductor can be viewed as an effective collision of the particle with its image charge (Figure 1). For the wavelengths long compare to the characteristic time of the collision process (wt<<1) the Fourier transform of the radiated magnetic field can be approximated as

$$\tilde{\mathbf{H}}(\omega) = \int_{-\infty}^{\infty} \mathbf{H}(t) e^{-i\omega t} dt \quad \int_{-\infty}^{\infty} \mathbf{H}(t) dt \tag{1}$$

Note that magnetic field in the integral is proportional to the full derivative of the field vector-potential $\mathbf{A}$, and therefore the spectral field produced by each particle in the collision can be written as[6]

$$\tilde{\mathbf{H}}(\omega) = \frac{1}{c}\left(\mathbf{A}_2 - \mathbf{A}_1\right) \times \mathbf{n} \ , \tag{2}$$

where $\mathbf{A}_1$ and $\mathbf{A}_2$ are the values of the vector potential before and after the collision, respectively. As the particle crosses the boundary of the conductor, its field is screened; hence, for the far field calculation we can assume that both a particle and its image counterpart come to a sudden stop, even though the real electron barely changes its velocity.

If the field of a charged moving particle far away from the source is given by the Liénard-Wiechert potential we obtain the expression for the spectral and angular distribution of the energy generated in the collision:

$$\frac{dE}{d\omega\ d\Omega} = \frac{e^2}{4\pi^2 c^3}\left(\frac{\mathbf{v}\times\mathbf{n}}{1-\frac{1}{c}\mathbf{n}\ \mathbf{v}} - \frac{\mathbf{v}'\times\mathbf{n}}{1-\frac{1}{c}\mathbf{n}\ \mathbf{v}'}\right)^2, \tag{3}$$

where **v**' is a velocity of the image charge. For the case of a 45° collision, Eq. (3) can be rewritten as

$$\frac{dE}{d\omega\ d\Omega} = \frac{e^2\beta^2}{4\pi^2 c}\left(\frac{\cos\theta}{1+\beta\sin\theta} - \frac{\sin\theta}{1-\beta\cos\theta}\right)^2, \tag{4}$$

where θ is defined relative to the specular reflection angle, which is in this case 90° with respect to the initial beam axis.

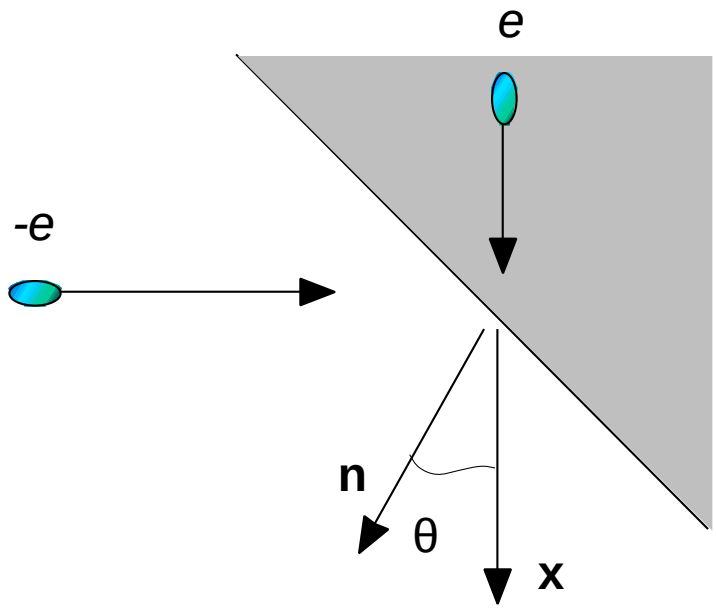

FIGURE 1. Transition radiation model for the far field analysis.

In the limit we have considered, where the metallic response is that of a perfect conductor, it can be seen that the angular distribution of the radiated energy does not depend on frequency. For the highly relativistic particle, the angular distribution is a narrow, slightly asymmetric double cone, centered around zero.

MACROBUNCH CTR MEASUREMENTS

Coherent Transition Radiation From a Bunched Beam

The total spectral energy $E_1(\omega)$ radiated by the single particle can be found by integrating Eq. (4) over all the observation angles. To find the transition radiation generated by a bunched beam of charged particles, we must add the fields due to the radiation of all the particles in the beam. For wavelengths long compare to the bunch length, the total field created by the particles is coherent, therefore for the total spectral energy, which is proportional to the square of the field, is $E(\omega) = N^2 E_1(\omega)$. However, as the wavelength approaches the size of the beam, this is no longer the case, and the total spectral energy radiated by the beam can be represented as

$$E(\omega) = |f(\omega)|^2 E_1 \ , \tag{5}$$

where $f(\omega)$ is a coherency function defined, for wavelengths long compared to the beam transverse width by the longitudinal beam profile $\rho(t)$. In the limit considered here, where the paraxial beam is much smaller radially than the relevant wavelengths (most beams of interest are "sausage shaped", being narrow compared to the longitudinal scale of interest), this function is

$$f(\omega) = \sum_{j=1}^{N} e^{i\omega t_j} \qquad N \int_{-\infty}^{\infty} \rho(t) e^{i\omega t} dt \ , \tag{6}$$

where $\rho(t)$ is normalized to unity. A notable violation of the assumption of negligible beam width occurs during the microbunch measurements, where the beam is wide compared to the CTR wavelengths, and a more general analysis is necesssary. For low frequencies of present interest, $|f(\omega)|^2$ converges to the expected value of N^2. Note that the expression on the right hand side Eq. (6) is the complex conjugate of the beam profile Fourier transform, and thus $f(\omega)$ is the population-weighted Fourier transform of the bunch longitudinal profile. Thus, in terms of the Fourier transform of the bunch profile, we can write

$$E(\omega) = 2\pi \tilde{E}_1 N^2 |\tilde{\rho}(\omega)|^2 \tag{7}$$

INTERFEROMETRIC MEASUREMENT OF CTR

The device shown in Figure 2 has been used to determine bunch lengths at UCLA[7] was built and developed at the University of Georgia by Prof. Uwe Happek. It is a polarizing Michelson interferometer based on beam splitters which use a transmission wire grid of 100 micron spacing. This spacing sets the upper limit on the spectral characteristics of the device.

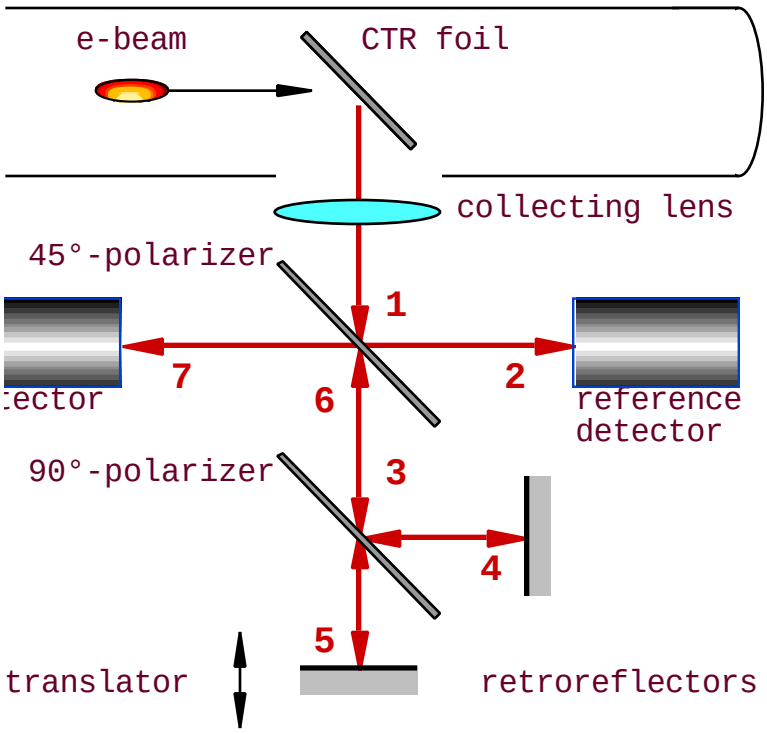

FIGURE 2. Interferometer device used to measure the CTR signal profile at UCLA.

The radiation is generated at a 45° CTR foil and exits the beam vacuum through a quartz window. It is gathered by the collecting lens {1}, then split equally by the first wire grid, which is oriented at 45° from vertical. Half of it is sent into the reference Golay cell detector {2}, which is used to normalize the signal in the detector at the end of the interferometer arm. The other half {3} is directed through the 90°-polarizer, where it is split back into horizontal (reflected) and vertical (transmitted) components {4-5}. Both are reflected at the end of their respective paths by retroreflectors and recombine at 45°-polarizer. The vertical polarization path {5} is adjusted by a motorized translator which allows variation of the relative paths of the vertically and horizontally polarized waves in increments of as small as 1.4 microns. Thus, as the polarized waves recombine at {6},

$$\mathbf{E}_6(\omega) \quad e^{i\omega t}\left(\hat{\mathbf{x}} - \hat{\mathbf{y}}e^{i\omega\tau}\right) = \frac{e^{i\omega t}}{\sqrt{2}}\left[\hat{\mathbf{e}}_+\left(1 - e^{i\omega\tau}\right) + \hat{\mathbf{e}}_-\left(1 + e^{i\omega\tau}\right)\right] \tag{8}$$

and only the $\mathbf{e}_+$ polarized fraction, whose amplitude depends on the position of the translator t, will be reflected from the polarizer and directed into the other Golay cell detector {7}. The result is an autocorrelation of the CTR signal: the total signal on the detector is effectively a combination of the signal and its t-delayed prototype. In that case, the Eq. (6) for $f(\omega)$ has to be modified:

$$\begin{aligned} f(\omega) &= \frac{1}{2\sqrt{2}} \sum_{j=1}^{N}\left(e^{i\omega t_j} - e^{i\omega(t_j+\tau)}\right) \approx \frac{N}{2\sqrt{2}} \int \rho(t) e^{i\omega t}\left(1 - e^{i\omega\tau}\right) dt \,, \\ \text{where} \quad |f(\omega)|^2 &= \frac{\pi N^2}{4}\,\tilde{\rho}^{\,*}(\omega)\tilde{\rho}(\omega)[1 - \cos(\omega\tau)] \,, \end{aligned} \tag{9}$$

and the total radiation energy received by the detector is

$$E_T = E_1 \int |f(\omega)|^2 d\omega \qquad \int \tilde{\rho}^{\,*}(\omega)\tilde{\rho}(\omega)[1 - \cos(\omega\tau)] d\omega \tag{10}$$

It is convenient at this point to examine the time domain picture again, by writing an explicit expression for one of the beam density Fourier transforms:

$$E_T \quad \int dt \rho(t) \int e^{i\omega t}\tilde{\rho}(\omega)\left(2 - e^{i\omega\tau} - e^{-i\omega\tau}\right) d\omega \tag{11}$$

It follows, that the only part of the total energy that changes with the delay t is an autocorrelation function of the beam density profile, or

$$E_T(\tau) \quad \int \rho(t)\rho(t+\tau) dt + \text{constant.} \tag{12}$$

Signal Analysis in the Frequency Domain

Even though the problem of extracting the beam density function from the integral in Eq. (12) has no unique solution, we can make certain assumptions about the beam shape and test them with respect to the measured results. The first, simplest, and most widely used *ansatz* is a Gaussian beam profile:

$$\rho(t) = \frac{1}{\sqrt{2\pi}\sigma_t} e^{-\frac{t^2}{2\sigma_t^2}} \tag{13}$$

In the case of many rf photoinjectors, it is motivated strongly by the nearly Gaussian shape of a photocathode drive laser pulse which governs the initial time profile of the emitted beam[7].

Using Eq. (14) one can see that the autocorrelation of such a beam, which can be found directly by measuring the detected energy as a function of the delay t, should give in return a Gaussian profile of width expanded by $\sqrt{2}$:

$$E_T(\tau) \quad e^{-\frac{\tau^2}{4\sigma^2}} + \text{constant.} \tag{14}$$

Autocorrelation measurements performed have been done for the electron beam in UCLA Saturnus photoinjector beamline, an example of which is shown in Figure 4; however, one can immediately see that the signal has positive and negative maxima. That can not be interpreted as an autocorrelation of Gaussian or any other form of the unipolar function.

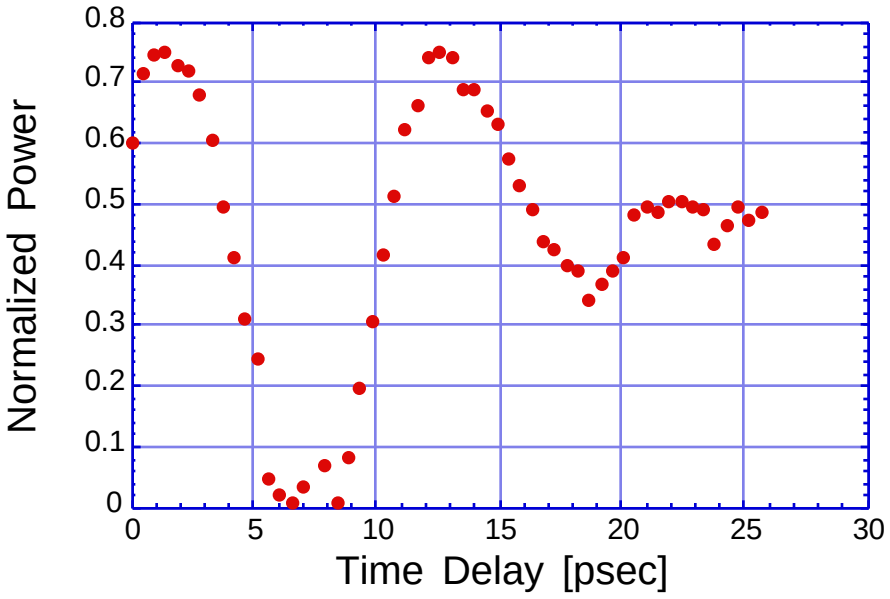

FIGURE 3. Normalized signal from Golay cell detector as a function of the translator position. Beam of ~200 pC at 13.25 MeV went through the 45° aluminum foil.

Indeed, according to Eq. 14, the most general autocorrelation signal measured in the time domain must be strictly unipolar if all of the information available at the radiation generation point is preserved. We can see that this is not in fact the case in the present UCLA measurements — as well as with previously reported CTR measurements[2]. To get a more accurate understanding of the autocorrelation signal structure in the time-domain, we have to revert to looking at the beam spectrum.

As was shown above, single particle radiation contains all the frequencies in the long wavelength limit with roughly uniform efficiency of generation out to the transverse dimensions of the foil. However, in the case of the very large wavelengths (more than a few mm), where the radiation is highly coherent and carries significant part of the total energy, the interferometer acts as a high-pass filter, due to diffractive losses as well as the physical apertures associated with the optics and detectors in the device. The Fourier transform of the measured signal, which is ideally Gaussian, displays such a filtering at low frequencies. We could in principle compensate for this filtering effect by restoring the low frequency components of the spectrum, by smoothly continuing the high frequency portion into a Gaussian shape peaked at zero frequency, as is traditionally done in this technique. For our measurements, however, this process gives unsatisfactory results, however, as the missing information is too significant. The restored profile always displays notable false artifacts; it is difficult to suppress the undulations in the profile which are in the raw autocorrelation[7]. To extract more meaningful information from our data we have therefore developed a more systematic frequency filtered model which can be used directly to fit the data in the time domain.

Time-Domain Fitting Approach

To proceed in constructing a useful model of what the frequency-filtered signal looks like in the time domain, we note first that the signal measured is in fact proportional to the autocorrelation of the filtered beam distribution function, an observation which allows an elegant and powerful formalism for model creation. We begin this analysis by introducing some analytical filter function of variable strength $g(\omega)$, which for ease of further analysis we take to be of the form

$$g(\omega) = 1 - e^{-\xi^2\omega^2} \quad , \tag{15}$$

which smoothly removes the low frequencies, with characteristic frequency cut-off ξ^{-1}. This form of the filter is physically motivated; it is obtained by the aperturing of a diffraction-limited transverse Gaussian-mode photon beam of uniform initial frequency spectrum in the far field, which is undoubtedly similar to our physical situation in this measurement..

We further assume that most of the low frequencies are attenuated before the signal arrives at the second polarizer; hence, the autocorrelation of the signal in the frequency domain is a product of a spectral beam density and the filter function $g(\omega)$

$$\tilde{\rho}_f(\omega) = \tilde{\rho}(\omega)\ g(\omega) \tag{16}$$

and the spectrum of the measured signal is

$$\tilde{s}(\omega) = \left|\tilde{\rho}_f(\omega)\right|^2 = \left|\tilde{\rho}(\omega)\right|^2\left[1 - 2e^{-\xi^2\omega^2} + e^{-2\xi^2\omega^2}\right] \tag{17}$$

Again assuming at this point *r(w)* to be a Fourier transform of a Gaussian beam, we obtain, using Parseval's theorem, an analytical expression for the signal in the time domain:

$$s(\tau) \quad \left[e^{-\frac{(\tau-\tau_0)^2}{4\sigma^2}} - \frac{2\sigma}{\sqrt{\sigma^2+\xi^2}}\, e^{-\frac{(\tau-\tau_0)^2}{4\left(\sigma^2+\xi^2\right)}} + \frac{\sigma}{\sqrt{\sigma^2+2\xi^2}}\, e^{-\frac{(\tau-\tau_0)^2}{4\left(\sigma^2+2\xi^2\right)}}\right]. \tag{18}$$

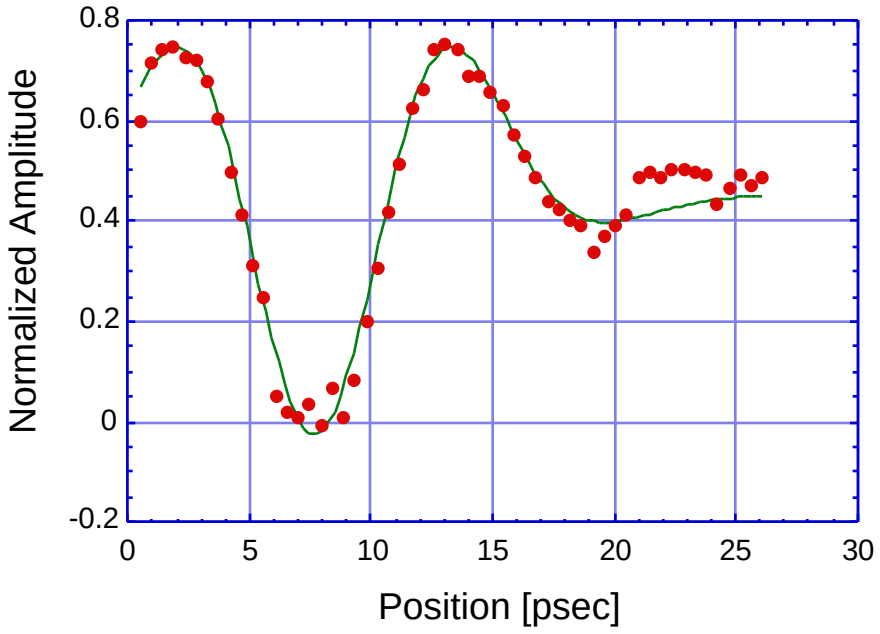

FIGURE 4. The fit $s(t)$ to the autocorrelated CTR signal.

This expression can be used to find the rms beam pulse length σ and, incidentally, the cut-off frequency of the interferometer, by a simple two parameter fit (σ, ξ) directly to our time-domain signal, without resorting to Fourier transformation of this data. On the average *z* was found very close to 1 psec, which correspond to the filter cut-off wavelength of 3 mm. An example of this fit is shown in Figure 4, in which it was determined that *s* ~2.8 psec, which is quite close to the injected photocathode drive laser *s* ~2.6 psec (also measured by autocorrelation, in the infrared, before quadrupling to convert the pulse to ultra-violet). It can be seen that the representation of the signal

by the sum of three Gaussians (one is the actual unfiltered autocorrelation peak, and the other two, arising from the missing frequency components, are broader, smaller in magnitude, and of alternating sign) gives an excellent fit to the data. The characteristic signature of this form is the existence of a central peak surrounded on both sides by two alternating sign local extrema — this signature is observed in all interferograms obtained in our CTR experiments. One should not always assume this to be the case, however. For example, a flatter profile formed by two overlapping Gaussians could have four, not two secondary extrema.

Analysis of the UCLA Measurements

Using the method described above, the number of interesting parametric studies have been performed and analyzed from the measurements made at UCLA[7]. The first consisted of measuring the dependence of the beam width on the charge Q, with the focusing solenoid and rf conditions held at optimum for minimized energy spread and transverse emittance. For the SASE FEL experiment at UCLA[8,9], the peak current in the beam was one of the crucial parameters which needed to be diagnosed under these conditions, and its dependence on charge was calculated using the measured $\sigma(Q)$. Another important parametric study performed was the examination of the beam pulse length as a function of the laser-induced injection phase in the rf gun. When the beam is injected so that it exits the gun ahead of the peak in the rf field, it is compressed longitudinally by the rf field gradient in both the gun, and to a lesser extent the linac. This effect was also observed using the CTR methods[7].

Up until this point we have assumed a simple Gaussian charge distribution. However, the fit function given does not cover some details in the signal. High frequency structure appears in the autocorrelation peaks in many of the measurements, indicating a fairly serious violation of the simple Gaussian model. For instance, the second (negative-going) sharp peak observed in Figure 7 at t=18.6 psec, well outside of the main signal, consistently appears in the data. This high frequency artifact in the signal cannot, of course, be generated by the low frequency filtering effect. This, along with a satellite off-momentum component of the distribution observed in momentum spectrum of the beam, led us to the conclusion that there is a satellite beam generated in the rf photocathode gun.

The effect of the satellite beam is particular well seen in the case of the compressed beam data. When the simple Gaussian model shown in Eq. (18) is used to fit the autocorrelation data, good agreement takes place only at the vicinity of the coincidence region. The mathematical formalism for the bi-Gaussian case is too extensive to be listed here; nevertheless it is fairly straightforward, following the same model as was used in the simple Gaussian case. As a result, the fit function generated provided the more accurate fit shown on Fig. 5. The beam profile deduced from the fit shows the

presence of the satellite beam 10 psec away from the main peak.

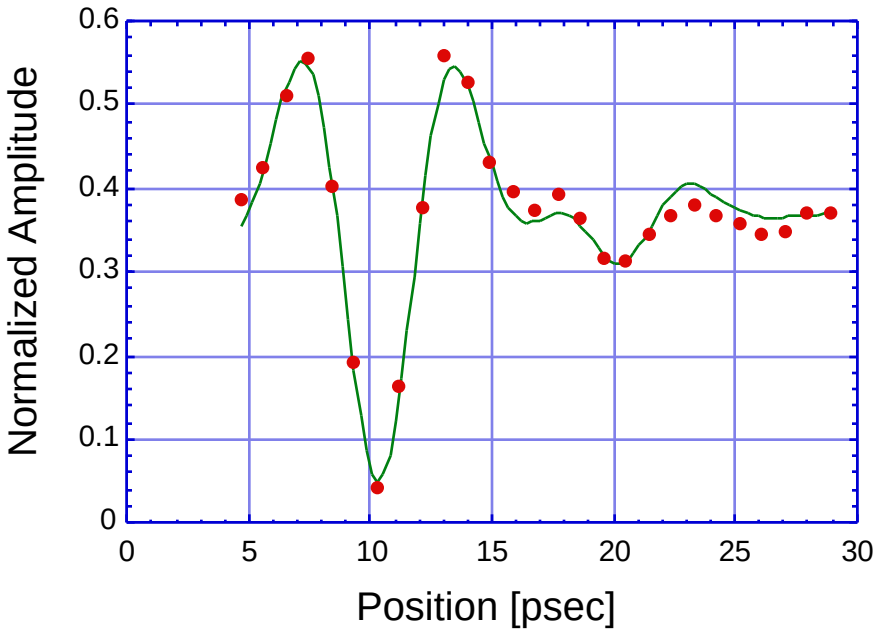

FIGURE 5. Two Gaussian time-domain filtered fit which takes the satellite beam into account.

MICROBUNCH CTR MEASUREMENTS

Microbunch-derived Coherent Transition Radiation

Charged particle beams with microbunch structure, the periodic modulation of the beam longitudinal profile, are now present in a variety of experimental scenarios, *e.g.* FELs[10], their inverse (IFELs)[11], and advanced accelerators based on laser excitation of plasmas and structures[12]. In the present experiments reported here, we focus on the microbunching that develops as a result of the self-amplified spontaneous emission FEL (SASE FEL) process[13]. This microbunching, which occurs at the wavelength of the FEL radiation, is central to the FEL gain process, as such a distribution produces radiation coherently, giving rise to exponential gain.

The traditional analysis of CTR which includes finite transverse profile and electron beam angular distribution effects, begins by writing the differential radiation spectrum due to multiparticle coherence effects as a function proportional to the single particle spectrum[14],

$$\frac{d^2U}{d\omega d\Omega} \quad N_b^2 F_L(\omega) F_T(\omega,\theta)\chi(\theta)\frac{d^2U}{d\omega d\Omega}\Big|_{\text{single e}^-}, \tag{19}$$

where N_B is the bunch population, $F_L(\omega)$ and $F_T(\omega,\theta)$ are the Fourier transform square amplitudes of the longitudinal (time) and transverse beam profiles, respectively. The factor $\chi(\theta)$ is due to the finite divergence of the beam and is usually taken to be close to unity. For narrow band transition radiation, however, this factor is not ignorable, as is discussed below.

The case of a microbunched beam produced, *e.g.* in an FEL or IFEL, has been worked out in detail in Ref. 5. Here we need to extend the previous results to account for possible asymmetries in the beam transverse distribution. The microbunched beam distribution is therefore taken to be

$$f(r,z) = \frac{N_b}{(2\pi)^{3/2}\sigma_x\sigma_y\sigma_z}\exp\left(-\frac{x^2}{2\sigma_x^2}-\frac{y^2}{2\sigma_y^2}-\frac{z^2}{2\sigma_z^2}\right)\left[1+\sum_{n=1}^{\infty}b_n\sin(nk_r z)\right], \tag{20}$$

where k_r is the radiation and, therefore, beam modulation wavenumber. Because the beam has Fourier components at k_r and its harmonics, an analysis following the methods of Ref. 5 predicts that the wave spectrum of CTR from the back of a 90 degree oriented foil is localized in peaks near these frequencies, with an angular spectrum of photon number at each peak $k = nk_r$ of

$$\frac{dN_\gamma}{d\theta} \quad \alpha\left(N_b b_n\right)^2 \frac{\sin^3(\theta)}{4\sqrt{\pi}nk_r\sigma_z\left(1-\beta\cos(\theta)\right)^2}\left[\exp\left(-\left(nk_r\sin(\theta)\right)^2\left(\sigma_x^2\sin^2(\varphi)+\sigma_y^2\cos^2(\varphi)\right)\right)\right]\chi(\theta), \tag{21}$$

where θ and φ are the polar and azimuthal angles with respect to the beam axis, respectively. Several predictions can be deduced from Eq. 21: first, familiarly the number of photons scales as the square of the number of radiators N_b^2. Also, the angular spectrum is narrowed considerably (when, as in the cases of present interest, $nk\sigma_{x,y}/\gamma > 1$) by the transverse geometric factor, which expresses the diffraction-limited (as opposed to the natural transition radiation angular distribution) of the coherent radiation, which for an axisymmetric beam of size σ gives a diffraction angle of $\theta_d = \left(\sqrt{2}nk_r\sigma\right)^{-1}$. This narrowing is a signature of coherence for the microbunched case, where the beam width is many wavelengths across. If we ignore the divergence factor ($\chi(\theta) \approx 1$), and perform the angular integration, we obtain a predicted number of

emitted photons at each harmonic (for forwad CTR, normal beam incidence),

$$N_\gamma \approx \frac{\alpha\left(N_b b_n\right)^2}{4\sqrt{\pi}k_r\sigma_z}\left(\frac{\gamma}{nk_r}\right)^4\left(\frac{\sigma_x^2+\sigma_y^2}{\sigma_x^3\sigma_y^3}\right), \tag{22}$$

which illustrates also the sensitive dependence of the CTR on beam dimensions. CTR is enhanced when the beam is dense, and there are many radiating electrons within a cubic half-wavelength.

Beam Energy	E	17.5 MeV
Peak Current	I	140 A
Charge/bunch	Q	1.5 nC
Bunch length (FWHM)	τ	11 psec
Energy spread	$\Delta\gamma/\gamma$	0.5%
Wiggler period	λ_W	2 cm
On-axis field	B_0	7.4 kG
FEL Wavelength	λ	13 μm
FEL parameter	ρ	0.008
Rms beam sizes	σ_x , σ_y	210, 160 μm

TABLE 1. Microbunch CTR experimental parameters

A measurement of some of these effects have been carried out at BNL[15], where a 0.3 nC electron beam was strongly bunched by the IFEL interaction with a 10.6 mm CO2 laser. The electron beam was not well focused at the foil (transverse beam size 0.6 by 5.5 mm), however, and so the CTR intensity was relatively weak. In order to measure CTR in this experiment, a large signal at the IFEL fundamental had to be suppressed, by looking at the forward radiation behind the opaque $d = 63$ μm Cu foil, and use of a high-pass filter. Theprimary result of this measurement was demonstration of a quadratic dependence of N_γ on N_b. Also, additional high-pass filters were used to establish CTR at or above the 4th IFEL harmonic. It is important that both effects have been previously established, as neither is easily seen in a SASE FEL experiment. The dependence $N_\gamma \sim N_b^2$ is not observable in a SASE experiment as the bunching factors b_n are gain and thus N_b dependent. In addition,

the $b_n \quad b_1^n$ are negligibly small unless the FEL is near saturation, which is not the case despite the high gain achieved in this experiment.

UCLA/LANL SASE FEL CTR Experiment

Because of the signal level, asymmetric beam, and calibration factors, the overall photon number was not given, nor compared to theoretical predictons for the BNL results. This exercise would have been problematic for the BNL case in any event, as scattering effects in the foil served to strongly suppress CTR production. Additionally, critical predictions of the microbunch CTR theory were not observed — the narrow-band frequency spectrum centered near the fundamental IFEL frequency and/or its harmonics, and the narrowing of the angular spectrum to the diffraction limit. Both of these attributes taken together indicate microbunching structure, meaning periodic longitudinal organization of the electrons. The BNL results indicate the presence of high frequency components, but do not strictly imply that the beam is organized into microbunches. In order to employ CTR as a method for diagnosing microbunching, all relevant aspects of the theory must be explored. The present measurements verify much of the theoretical model, and give some insight into the microbunching process in a high-gain SASE FEL.

The present experiments[16] were performed by a UCLA/LANL collaboration at the AFEL facility at Los Alamos National Laboratory, a 1300 MHz rf photoinjector which produces a 100-bunch train of low-emittance, high current electron bunches. The experimental setup is shown in Fig. 1, and the beam parameters relevant to this experiment, measured using the methods described in Ref. 17, are given in Table 1. The undulator used was the 2 m UCLA/Kurchatov[9] device employed in recent high-gain SASE FEL experiments; its parameters are also in displayed in Table 1. The 6 μm thick Al CTR foil was mounted on an insertable actuator normal to the beamline, 1 cm after the undulator exit, in a large opaque stop, to eliminate all FEL radiation when the foil is inserted. This placement of the foil allowed us to collect FEL and CTR radiation alternatively in the same optical beamline, as the object point in both cases is nearly the same. In addition, the beam defocuses transversely in 21 cm, and space charge effects are predicted to debunch the beam in roughly 50 cm from the end of the undulator[18]. These effects are avoided in our geometry. The optical beamline was set so that only diffraction limited coherent radiation passes the acceptance angle $\theta_{acc} \approx 12$ mrad, be collected and focused into the HgCdTe detector. The incoherent TR, however, with its angular peak at $\theta_{\mathrm{inc}} \approx \gamma^{-1} = 29$ mrad, is collected with only a few percent efficiency. The detector provides an equilibrium output signal level proportional to the radiated energy per electron pulse, with the proportionality constant obtained from a calibrated laser power meter.

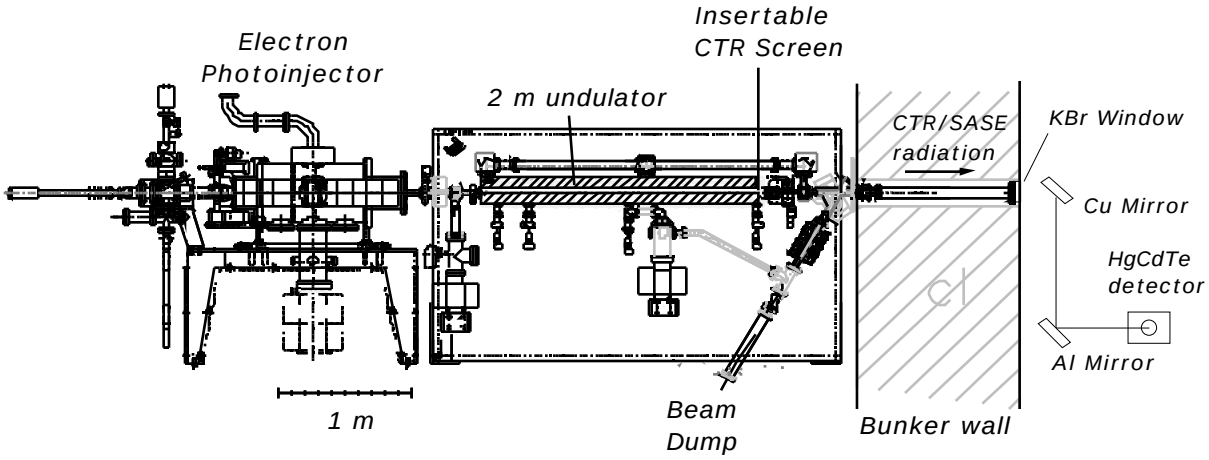

FIGURE 6. Electron injector, undulator, and CTR/SASE optical beamline at LANL AFEL facility.

The conditions of high SASE FEL gain with a 1.5 nC beam seen in Ref. 17 were reestablished for this experiment. The performance of the FEL was optimized by setting the beam focus at the matched condition at the undulator resonance, and fine-tuning the rf phase of the photoinjector. This procedure gave highest SASE output at relatively low injection phase, which corresponds to higher dynamical compression of the electron bunch, and thus higher peak current, FEL gain, and microbunching effect. After insertion of the foil, however, in addition to incremental changes in solenoid focusing, it was found that a small adjustment (2-3 degrees) of the rf phase was necessary to maximize in the CTR signal, as is shown in Figure 7. As the rf accelerating wave provides phase dependent focusing[19], this adjustment (which has a negligible effect on the final energy of the beam) serves to minimize the beam size attainable at the foil, thus optimizing the CTR production (*cf.* Eq. 4). The SASE signal is less sensitive to beam focusability, however, as the gain in this experiment is dominated by diffraction, which is mitigated with larger $\sigma_{x,y}$[20]. The peak regions of the SASE and CTR signals as a function of rf phase overlap, as they must, because the CTR is dependent on the SASE-induced bunching. In our case, using the analysis of Ref. 17, the measured gain was near 10^5. The bunching predicted for these conditions by the 3-D FEL simulation code GINGER, for a range of parameters corresponding to experimental uncertainties, was $b_1 = 0.008\text{-}0.01$, with negligible bunching at the higher harmonics.

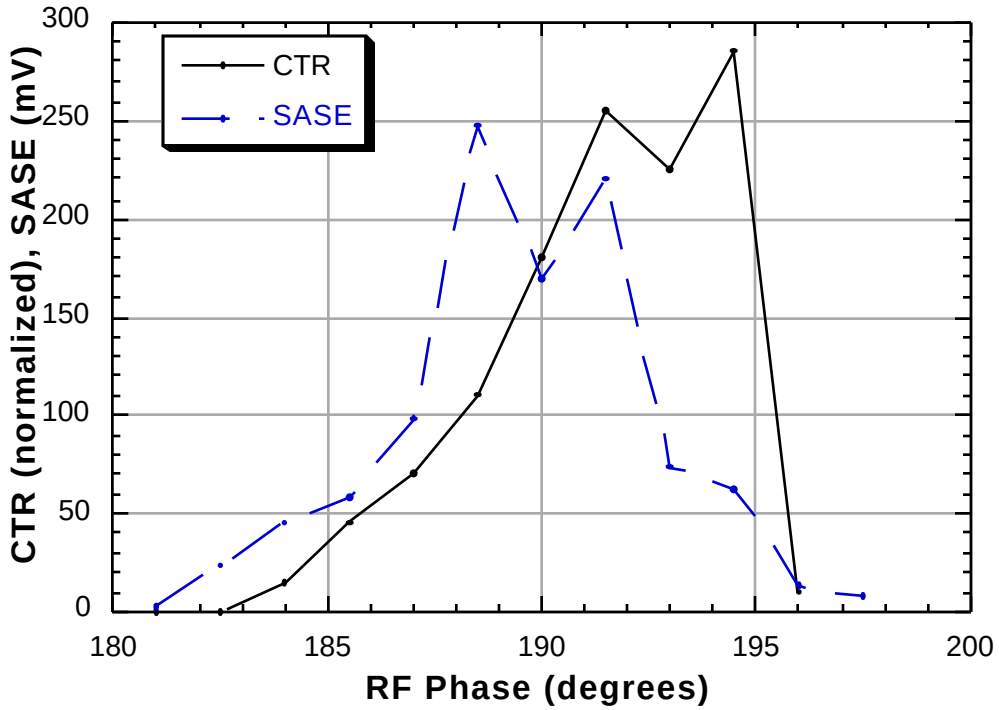

FIGURE 7. SASE and CTR signals as a function of rf phase, with CTR scaled to SASE amplitude.

Before discussing the data further, we remark that initially the CTR measurements were attempted with a 50 μm Al foil, with the result that the CTR signal was weaker than expected, leading us to examine the effects of foil scattering. For an uncorrelated gaussian phase space distribution typical of a scattered beam, a formalism has been developed[14] to evaluate $\chi(\theta)$. Several results of this analysis can be described. First, $\chi(\theta)$ is near unity for small angles when the angular spread of the incoherent radiation is large compared to the rms beam divergence, $\sigma' \quad \theta_{scat} << \gamma^{-1}$. If this condition is violated, $\chi(\theta)$ diminishes rapidly. After subsitution of the correct form of $\chi(\theta)$ into Eq. 3 and integrating, we can define a factor $\eta(\gamma\sigma')$ (keeping all other parameters constant) which indicates the degree of suppression of the CTR signal due to beam divergence. Note that since the scattering angle $\theta_{scat} \quad \gamma^{-1}d^{1/2}$, η is independent of γ and is a function only of foil material and thickness. For our 50 μm Al foil, where $\theta_{scat} \approx \gamma^{-1}$, $\eta \quad 0.11$, and for the highly scattered BNL case $\eta \quad 5 \times 10^{-3}$. In order to avoid this effect, we need $\theta_{scat} << \gamma^{-1}$, which was achieved by using the 6 μm Al foil. Integrating Eq.20, and multiplying by the factor $\eta = 0.61$ for our case yields a

photon number per electron pulse, for the range of GINGER-predicted b_1 and other beam parameters given in Table 1, of $N_\gamma = 2.8 - 4.4 \times 10^8$. The measured photon number per pulse at the peak given in Fig. 2 is $N_\gamma = 3.5 \times 10^8$. The theory, simulation and experiment thus agree to within experimental and simulational uncertainty.

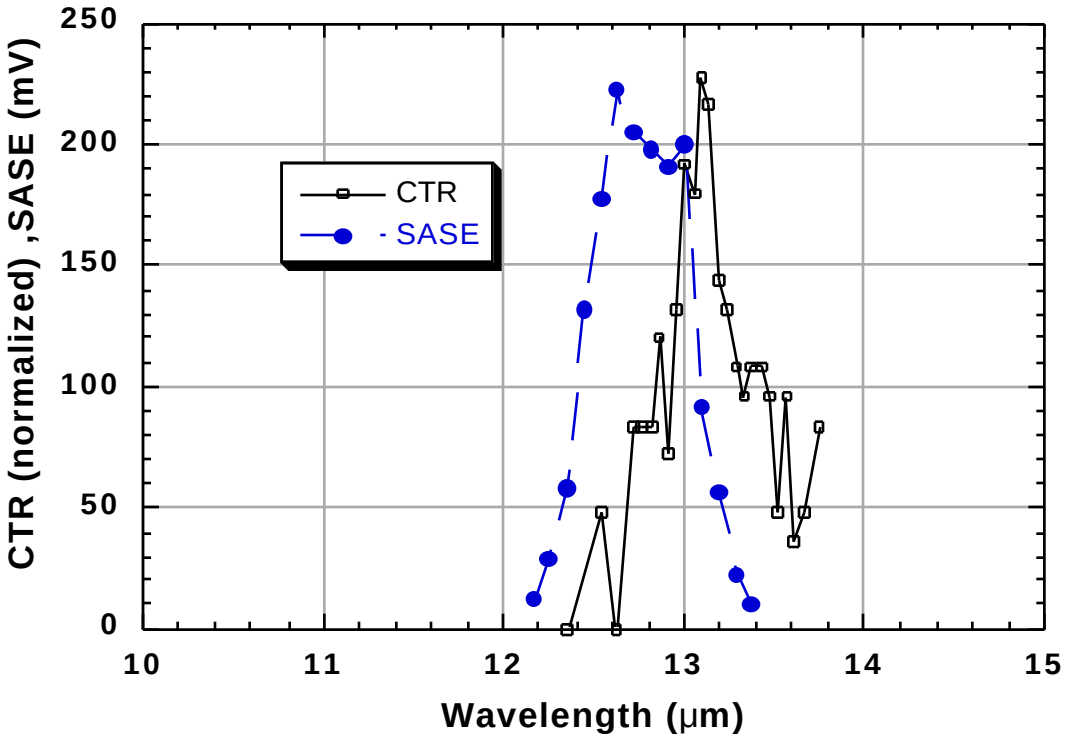

FIGURE 8. SASE and CTR signals as a function of wavelength as measured with monochromator, with CTR scaled to SASE amplitude.

Having established an optimization procedure for both SASE and CTR, we then undertook a spectral study of both signals by sending them through a Jerrell Ash monochromator. In order to maximize the signal through the monochromator its input collimating slits were removed, which resulted in a measured (by comparing the SASE line-width with and without the slits) intrinsic resolution of 0.177 μm . The SASE and CTR spectra thus obtained (with the SASE attenuated by a factor of 3 and the CTR multiplied by 10 to give similar scale), are shown in Fig. 3. Both the CTR and SASE signals are both localized near the same wavelength, with a small difference in the distribution centers. This discrepancy points to an inadequacy in the standard analysis of CTR[5,14]. Because the radiation components are summed by considering a temporal "snap-shot" of the beam distribution[14], possible off-axis shifting of the wave-length spectrum of the radiation, which is not created "at rest" by the foil, but over a radiation

formation length[21] by the relativistic electrons, cannot be obtained. A simple calculation of energy exchange between the initially radiated wave and the microbunched beam electrons indicates that for small angles, the off-axis wavelength spectrum is shifted in analogy to the FEL shift, $\lambda \rightarrow \lambda\left(1+(\gamma\theta)^2\right)$. While the SASE radiation is peaked at $\theta = 0$, the CTR is peaked off-axis, leading to a shift in the centroid of CTR wavelength with respect of SASE by $\Delta\lambda/\lambda \quad (\gamma/2k_r\sigma)^2 \quad 3.8\%$; the observed shift is 3.3%.

In conclusion, we have demonstrated two critical aspects of the microbunching-induced coherent transition radiation — the narrowing of the angular spectrum, and the formation of line structure in the wavelength spectrum. These observations have verified some aspects of microbunching-induced CTR theoretical analysis, but challenged others. In particular, this analysis must be redone employing a travelling beam model, and not the stationary model which is presently used[8,9]. Also, in order to have a well understood diagnostic, which produces the expected level of coherence, one must minimize the beam divergence induced by the CTR interaction (foil scattering). It should be emphasized that this diagnostic method is important not only for FEL experiments but for short wavelength advanced accelerator experiments, such as the plasma accelerators[22], cathodeless, plasma-based injectors[23], and direct laser acceleration.

It is equally useful to view the current experiments from the FEL physics view point, as these measurements were performed at a SASE FEL exit, verifying the crucial role that microbunching plays in the gain process. The narrow angular spread of the CTR signal indicates that the microbunching is fairly uniform in the transverse dimension; otherwise, the CTR signal would be have a less localized angular spectrum. Also, the agreement of measured and predicted photon number, using the microbunching given by simulations, is especially encouraging, as it provides an independent check, in addition to the FEL radiation output, on the code predictions. The CTR microbunching method will be even more useful in the next generation SASE FEL experiments, in which the FEL should saturate. In this case the signal will be larger, not only on the fundamental radiation wavelength, but on the harmonics as well. The large signal levels will allow closer investigation of off-axis Doppler shift effects (direct measurement of the CTR angular/frequency correlations). The added information from harmonics should permit a more detailed reconstruction of the beam's microbunched distribution.

REFERENCES

1. U. Happek, A.J. Sievers and E.B. Blum, *Phys. Rev. Lett.* **67** (1991) 2962.

2 . H.-C. Lihn, P. Kung, C. Settakorn, and H.Weidemann, *Phys. Rev. E* **53** (1996) 6413.

3 . Y. Shibata, *et al., Phys. Rev. E* **50** (1994) 1479.

4 . R.Lai and A.J. Sievers, *Phys. Rev. E* **52** (1995) 4576.

5. J. B. Rosenzweig, G. Travish and A. Tremaine, *Nucl. Instrum. Meth. A* **365**, 255 (1995)

6 . Landau, L.D. , *The classical theory of fields* p. 196 (Addison-Wesley, 1951).

7. A. Murokh, *et al., Nucl. Instr. and Methods A.* **410**, 452 (1998)

8. G. Travish, UCLA PhD thesis (UMI Dissertation Services, #9704598, Ann Arbor, 1996)

9. M. Hogan, *et al., Physical Review Letters* **80**, 289 (1998).

10. R. Bonifacio, C. Pellegrini, and L. Narducci, *Optics Comm.* **50,** 373 (1984).

11. A. Van Steenburgen, *et al.*, *Phys. Rev. Lett.* **80**, 289 (1998).

12. J. Rosenzweig, *et al., Phys. Rev. Lett.***74**, 2467 (1995).

13. R. Tatchyn *et al., Nucl. Instrum. Meth. A* **375**, 274 (1996), C. Pellegrini, *et al., Nucl. Instr. Methods A* **331**, 223 (1993), J. Rossbach et al., *Nucl. Instr. and Meth.* **A375**, 269 (1997).

14. Yukio Shibata, *et al., Phys. Rev. E* **50**, 1479 (1994)

15. Y. Liu, *et al., Phys. Rev. Lett.* **80**, 4418 (1998); Y. Liu, PhD thesis, UCLA Dept. of Physics and Astronomy (1997).

16. A. Tremaine, *et al.,* submitted for publication to *Phys. Rev. Lett*.

17. M. Hogan *et al.,* accepted for publication in *Phys. Rev. Lett.* SASE FEL gain in excess of 10^5 was first seen in this experiment.

18. J. Rosenzweig, *et al., Nucl. Instr. Methods A* **393**, 376 (1997).

19. S. Reiche, *et al., Phys. Rev. E* **56**, 3572 (1997).; J. Rosenzweig and L. Serafini, *Phys. Rev. E* **49**, 1499 (1994).

20. E. Saldin, V. Schneidmuller and M. Yurkov, *Optics Comm.* **97**, 272 (1993).

21. L. Warstki, *et al., J. Appl. Phys.*. **46**, 3644 (1975).

22. C.E. Clayton, *et al., Phys. Rev. Lett.* **70**, 37 (1993).

23. D. Umstadter, J. K. Kim and E. Dodd, *Phys. Rev. Lett.* **76**, 2073 (1996).